Nitric Oxide 92 (2019) 18–25

Contents lists available at ScienceDirect

Nitric Oxide

journal homepage: www.elsevier.com/locate/yniox

S-Nitrosoglutathione exhibits greater stability than *S*-nitroso-*N*-acetylpenicillamine under common laboratory conditions: A comparative stability study

Alyssa C. Melvin[a], W. Matthew Jones[a], Alec Lutzke[a], Christopher L. Allison[a], Melissa M. Reynolds[a,b,c,*]

[a] *Department of Chemistry, Colorado State University, Fort Collins, CO, 80523, USA*
[b] *School of Biomedical Engineering, Colorado State University, Fort Collins, CO, 80521, USA*
[c] *Chemical and Biological Engineering, Colorado State University, Fort Collins, CO, 80521, USA*

ARTICLE INFO

Keywords:
S-nitrosothiol
S-Nitrosoglutathione
S-Nitroso-*N*-Acetylpenicillamine
Nitric oxide
Stability
Decomposition

ABSTRACT

S-Nitrosothiols (RSNOs) such as *S*-nitrosoglutathione (GSNO) and *S*-nitroso-*N*-acetylpenicillamine (SNAP) are susceptible to decomposition by stimuli including heat, light, and trace metal ions. Using stepwise isothermal thermogravimetric analysis (TGA), we observed that NO-forming homolytic cleavage of the S–N bond occurs at 134.7 ± 0.8 °C in GSNO and 132.8 ± 0.9 °C in SNAP, contrasting with the value of 150 °C that has been previously reported for both RSNOs. Using mass spectrometry (MS), nuclear magnetic resonance (NMR), and attenuated total reflectance Fourier transform infrared spectroscopy (ATR-FTIR), we analyzed the decomposition products from TGA experiments. The organic product of GSNO decomposition was glutathione disulfide, while SNAP decomposed to form *N*-acetylpenicillamine disulfide as well as other products, including tri- and tetrasulfides. In addition, we assessed the relative solution stabilities of GSNO and SNAP under common laboratory conditions, which include variable temperature, pH, and light exposure with rigorous exclusion of trace metal ions by chelation. GSNO exhibited greater stability than SNAP over a 7-day period except in one instance. Both RSNOs demonstrated an inverse relationship between solution stability and temperature, with refrigeration considerably extending shelf life. A decrease in pH from 7.4 to 5.0 also enhanced the stability of both RSNOs. A further decrease in pH from 5.0 to 3.0 resulted in decreased stability for both RSNOs, and is notably the only occasion in which SNAP proved more stable than GSNO. After 1 h of exposure to overhead fluorescent lighting, both RSNOs displayed high susceptibility to light-induced decomposition. After 7 h, GSNO and SNAP decomposed 19.3 ± 0.5% and 30 ± 2%, respectively.

1. Introduction

S-Nitrosothiols (RSNOs) represent attractive substrates for the controlled delivery of nitric oxide (NO), a radical species that participates in a variety of physiological processes such as vasodilation, immune response, and cell signaling [1]. In the development of antithrombotic biomaterials, RSNOs serve as NO donors in polymer formulations used to fabricate blood-compatible biomedical devices [2–8]. Other applications use RSNOs as a convenient NO source in biological research where the cytotoxic properties of NO can be exploited for antimicrobial effects, treatment of cancer, or as a method of eliciting unique biochemical responses [9–11]. NO release from RSNOs can be triggered through physical and chemical stimuli including heat, visible and ultraviolet light, and exposure to transition metal ions (most notably copper) [12–14]. During handling, preparation, and usage, RSNOs can be exposed to stimuli that initiate their decomposition [15]. As a consequence of this instability, appropriate precautions are necessary to limit premature RSNO decomposition. This consideration is particularly critical in sensitive biological applications where reliable delivery of NO from RSNO substrates may not be achievable without careful control of environmental factors.

Two commonly used RSNOs are *S*-nitrosoglutathione (GSNO), a bioavailable primary RSNO in mammalian blood, and *S*-nitroso-*N*-acetylpenicillamine (SNAP), a synthetic tertiary RSNO derived from the amino acid penicillamine (Fig. 1a and b) [2–8,16–18]. These RSNOs are reported to exhibit sufficient stability as solids to permit handling and

* Corresponding author.
E-mail address: melissa.reynolds@colostate.edu (M.M. Reynolds).

https://doi.org/10.1016/j.niox.2019.08.002
Received 12 April 2019; Received in revised form 20 May 2019; Accepted 6 August 2019
Available online 06 August 2019
1089-8603/

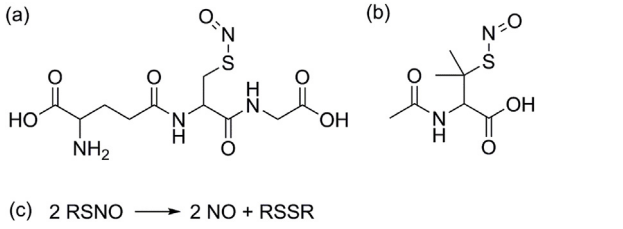

Fig. 1. (a) *S*-Nitrosoglutathione (GSNO), (b) *S*-nitroso-*N*-acetyl-penicillamine (SNAP), (c) *S*-nitrosothiol (RSNO) decomposition.

storage for prolonged periods of time [14]. It has been proposed that NO release from RSNOs occurs through homolytic cleavage of the S–N bond to form NO and thiyl radicals, and the latter product may dimerize to form the corresponding disulfide (Fig. 1c). Homolytic S–N bond dissociation energies are estimated to fall within the range of 20–32 kcal mol^{-1}, which encompasses half-lives of minutes to years [15,19,20].

Despite their frequent use as NO donors, there is limited and conflicting literature examining the comparative stability of GSNO and SNAP. Existing literature indicates that tertiary RSNOs are more stable than their primary counterparts [21–24]. There is also literature suggesting that GSNO is an exception to this trend [2]. However, other research has shown that both RSNOs thermally lyse NO near 150 °C, indicating that the strength of the S–N bonds are equivalent despite substitution differences [25].

Herein, we investigated these discrepancies using stepwise isothermal thermogravimetric analysis (TGA). The decomposition products obtained from TGA experiments were characterized by mass spectrometry (MS), nuclear magnetic resonance (NMR), and attenuated total reflectance Fourier transform infrared spectroscopy (ATR-FTIR). Furthermore, the solution stability of GSNO and SNAP was investigated as a function of temperature, pH, and light exposure in the presence of a metal ion chelator using ultraviolet–visible spectroscopy (UV–Vis) with the goal of establishing proper handling, preparation, and usage techniques.

2. Materials and methods

2.1. Chemicals and reagents

The following chemicals and reagents were used as received: acetone (99.5%, Sigma-Aldrich), *N*-acetyl-D-penicillamine (NAP; 99.0%, Sigma-Aldrich), citric acid monohydrate (ACS certified, Fisher), deuterium oxide (99.9% D, Cambridge Isotopes Laboratories), dinitrogen (ultra-high purity, Airgas), ethylenediaminetetraacetic acid disodium salt dihydrate (EDTA; 99.0%, Sigma-Aldrich), L-glutathione, oxidized (GSSG; 98%, Sigma-Aldrich), glutathione, reduced (GSH; 98%, AMRESCO), helium (ultra-high purity, Airgas), hydrochloric acid (35.0–38.0 wt %, Fisher), magnesium sulfate (98.0%, EMD), methanol (99.9%, Fisher), methanol-d_4 (99.8% D, Cambridge Isotope Laboratories), nitric acid (68.0–70.0 wt %, EMD), phosphate-buffered saline (PBS) tablets (Biotechnology grade, AMRESCO), sodium hydroxide (98.9%, Fisher), sodium nitrite (97.0%, EMD; 99.999%, Alfa-Aesar), sodium phosphate dibasic (anhydrous, 99.0%, Sigma-Aldrich), and sulfuric acid (95.0–98.0 wt %, BDH/VWR International). Ultrapure water (18.2 MΩ cm) was prepared using a Millipore Direct-Q water purification system (EMD Millipore).

2.2. Synthetic methods

S-Nitroso-N-acetyl-penicillamine: In a typical reaction, *S*-nitroso-*N*-acetyl-penicillamine (SNAP) was prepared following an adapted protocol of the method reported by Field et al. [26]. A solution of methanol (10 mL) and 1 M hydrochloric acid (10 mL) was prepared and cooled to 0 °C using an ice-water bath. Concentrated sulfuric acid (1 mL) was added to the solution. *N*-Acetyl-D-penicillamine (NAP; 0.956 g, 5.0 mmol) was added to the solution while stirring, resulting in a NAP suspension. Separately, sodium nitrite (0.690 g, 10.0 mmol) was dissolved in ultrapure water (5 mL), and this solution was sequentially added in small portions to the NAP suspension, resulting in vigorous bubbling and development of a green color for the mixture. The reaction was immediately shielded from light and stirred for 40 min at room temperature. The resulting mixture was filtered to isolate a green precipitate, which was subsequently washed with 4 × 10 mL of 0–5 °C ultrapure water. The product was placed under dynamic vacuum (< 100 mTorr) for 4 h to remove residual solvent, affording 0.594 g of SNAP (54% yield, 97% pure). The product was stored in a light-free, −20 °C freezer when not in use. ^{1}H NMR (400 MHz, CD_3OD): 5.32 (m, 1H), 2.04 (s, 3H), 2.01 (s, 3H), 1.97 ppm (s, 3H) [27]. ^{13}C NMR (101 MHz, D_2O): 174.70, 173.47, 61.49, 57,77, 26.65, 25.17, 22.26 ppm. UV–Vis (H_2O): 339 nm ($\pi \rightarrow \pi^*$), 591 ($n_N \rightarrow \pi^*$) [13].

S-Nitrosoglutathione: In a typical reaction, *S*-nitrosoglutathione (GSNO) was prepared following an adapted protocol of the method reported by Hart [28]. Reduced glutathione (1.54 g, 5.0 mmol) was suspended in ultrapure water (8 mL) and dissolved with the addition of 2 M hydrochloric acid (2.5 mL). The reaction was cooled to 0 °C using an ice-water bath, and sodium nitrite (0.345 g, 5.0 mmol) was added. The reaction was immediately shielded from light and stirred for 40 min at 0 °C. The resulting mixture was filtered to isolate a reddish-pink precipitate, which was subsequently washed with 5 × 5 mL of 0–5 °C ultrapure water and 3 × 5 mL of acetone. The product was placed under dynamic vacuum (< 100 mTorr) for 4 h to remove residual solvent, affording 0.865 g of GSNO (51% yield, 98% pure). The obtained product was stored in a light-free, −20 °C freezer when not in use. ^{1}H NMR (400 MHz, D_2O): 4.70–4.61 (m, 1H), 4.20–3.90 (m, 2H), 3.93 (s, 2H), 3.78 (t, 1H, J = 6.4 Hz), 2.42 (t, 2H, J = 7.6 Hz), 2.18–2.01 (m, 2H) [29]. ^{13}C NMR (101 MHz, D_2O): 175.27, 174.04, 174.01, 172.42, 54.28, 53.14, 42.08, 34.03, 31.69, 26.49 ppm. UV–Vis (H_2O): 335 nm ($\pi \rightarrow \pi^*$), 545 nm ($n_N \rightarrow \pi^*$) [28].

2.3. Physical methods and instrumentation

Sample handling: Experimental techniques and sample handling were performed on the benchtop or on a dual-manifold Schlenk line using N_2 in the inert gas manifold.

Thermal analyses: Stepwise isothermal thermogravimetric analyses (TGA) were performed using a TA Instruments TGA Q500 instrument equipped with a standard ceramic furnace. Stepwise isothermal thermogravimetric analyses with coupled mass spectrometry (TGA-MS) were performed using a TA Instruments TGA Q500 instrument equipped with an Evolved Gas Analysis (EGA) quartz-lined furnace coupled to a Discovery Mass Spectrometer. For the standard ceramic furnace, ultra-high purity (UHP) N_2 was used as the purge gas at a flow rate of 40 mL min^{-1} for the balance purge and 60 mL min^{-1} for the furnace purge. For the EGA furnace, ultra-high purity (UHP) helium was used as the purge gas at a flow rate of 10 mL min^{-1} for the balance purge and 90 mL min^{-1} for the furnace purge. Samples (5–10 mg) were contained in platinum sample pans. Stepwise isothermal heating was programmed as follows: ramp 10 °C min^{-1} to 100 °C, stepwise isothermal ramp at 2 °C min^{-1} to 145 °C with isotherm entry-exit values of % wt. change/min at 0.4% min^{-1}, isothermal 1000 min until entry-exit condition met or 145 °C reached, return to stepwise isothermal ramp conditions.

NMR analyses: Nuclear magnetic resonance (NMR) spectroscopy was performed using a Bruker AVANCE NEO 400 spectrometer to observe ^{1}H and ^{13}C nuclei. In ^{1}H NMR experiments, samples were dissolved in deuterium oxide (D_2O) or methanol-d_4 and spectra were acquired at 400 MHz from 32 transients at 25 °C. Chemical shifts were referenced to the solvent peak (HDO; 4.790 ppm). In ^{13}C NMR experiments, samples were dissolved in D_2O and spectra were acquired at 101 MHz from 512

transients at 25 °C. Methanol (49.50 ppm) was added to the D_2O as an internal reference at a concentration of 1 μL mL^{-1}.

ATR-FTIR analyses: Attenuated total reflectance Fourier transform infrared spectroscopy (ATR-FTIR) was performed using a Nicolet iS50 FTIR spectrometer equipped with an ATR sampling accessory with a diamond crystal. Representative spectra are shown for ATR-FTIR data.

Solution stability studies: Glassware was cleaned using aqua regia and ultrapure water. All RSNO solutions (20 mL) were prepared at 1.5×10^{-3} M with 100 μM EDTA under aerobic conditions and shielded from light in 20 mL amber scintillation vials. Temperatures sampled were 5 °C, 22 °C, and 37 °C in 10 mM PBS (pH 7.4). Solutions of pH 3.0 (0.12 M) and pH 5.0 (0.15 M) were prepared in citric acid-sodium phosphate dibasic buffer. Solution stability under fluorescent light exposure was performed in a fume hood with a light-to-benchtop distance of 122 cm. The intensity of the fume hood light was reported at 861 lux (2.4 m candles) by the manufacturer (Bedcolab).

UV–Vis analyses: RSNO decomposition was measured by ultraviolet–visible (UV–Vis) spectroscopy in 1.0 cm quartz cuvettes using a Nicolet Evolution 300 UV–Vis spectrophotometer.

Light spectrum analysis: Laboratory light spectra were acquired using an Ocean Optics STS-UV microspectrometer with a 400 μm QP400-2-SR optical fiber.

MS analyses: Mass spectra were obtained using an Agilent 6224 time-of-flight mass spectrometer (TOF-MS) equipped with a dual electrospray ionization source operated in negative ion mode using a 100% methanol mobile phase.

Data reporting and statistical analysis: All data were reported as a mean ± standard deviation of $n \geq 3$ replicate measurements. Statistical difference was determined using two-tailed Student's t-test ($p < 0.01$). Thermal decomposition temperatures were determined using the Onset Point analysis function with the TRIOS (v. 4.2.1.36612, TA Instruments) software platform. Percent RSNO remaining in solution was determined by monitoring the decomposition via decreasing absorption at λ_{max} (GSNO, 335 nm; SNAP, 339 nm). The absorption at time t (A_t) was compared to the initial absorbance at t_0 (A_{t0}) by the equation: $(A_t/A_{t0})\cdot 100\%$.

3. Results and discussion

3.1. Thermal stability of solid GSNO and SNAP

RSNOs possess modest thermal stability with bond dissociation energies reported in the range of 20–32 kcal mol^{-1} [19,20]. Thermal scission of the S–N bond is believed to proceed through homolytic dissociation, resulting in the formation of NO and the corresponding thiyl radical (Fig. 1c) [13]. We examined the thermal stability of solid GSNO and SNAP using stepwise isothermal TGA to determine the temperature at which NO is released (Fig. 2). Our results indicate that GSNO and SNAP decompose at 134.7 ± 0.8 °C and 132.8 ± 0.9 °C, respectively. These decomposition temperatures are substantially lower than previously published values obtained by thermal methods. For example, Bainbrigge et al. reported that both GSNO and SNAP decompose at 148 °C, while Parent et al. found that the NO-forming decomposition of GSNO occurs at 150.3 °C [25,29]. We observed that routine variation in purity and age of RSNO samples is insufficient to account for this 15 °C difference in decomposition temperature. For example, we found that low-purity (81%) GSNO decomposed at 138.0 ± 0.1 °C, overestimating the decomposition temperature by approximately 3 °C. The discrepancy in the temperature may be due to the rapid heating of the sample (e.g., > 10 °C min^{-1} in common furnace configurations) during TGA resulting in substantial overestimation of temperatures at which thermal phenomena are resolved [30]. We hypothesize that this overestimation is minimized by our heating rate of 2 °C min^{-1}, and that the actual thermal decomposition temperatures of GSNO and SNAP are lower than previously reported [25,29].

Thermal decomposition of GSNO (336.32 g mol^{-1}; $C_{10}H_{16}N_4O_7S$) resulted in a weight decrease of 9.3 ± 0.1%, which is largely consistent with the theoretical 8.9% reduction in mass expected from stoichiometric loss of NO. Thermogravimetric analysis coupled with mass spectrometry (TGA-MS) was used to evaluate the gaseous products evolved during the thermal decomposition of GSNO. At 134 °C, species of 30 m/z were rapidly released, consistent with the production of NO (Supplementary Fig. 1). GSNO TGA experiments were halted at 145 °C and cooled to ambient temperature inside the furnace (UHP N_2, light-free) for further analysis by ATR-FTIR and ^{1}H NMR. Over the course of the thermal experiments, GSNO transitioned from a light pink powder to an off-white powder that remained soluble in water. The ATR-FTIR spectra (Supplementary Fig. 2) show the disappearance of the diagnostic NO band at 1477 cm^{-1} (N═O stretching mode), supporting the absence of the RSNO functional group in the organic decomposition product [13]. Analysis by ^{1}H NMR reveals that the decomposition product is clearly distinct from GSNO and is consistent with commercial GSSG (Fig. 3). These findings, in addition to the TGA data, support that thermal decomposition of GSNO yields GSSG and NO stoichiometrically according to the scheme depicted in Fig. 1c [25].

In contrast, SNAP (220.24 g mol^{-1}; $C_7H_{12}N_2O_4S$) experienced a 15.2 ± 0.6% decrease in weight following TGA experiments, modestly exceeding the theoretical value of 13.6% that corresponds to exclusive loss of NO. This discrepancy may indicate that thermal decomposition of SNAP or SNAP products is not limited to homolytic cleavage of the S–N bond and subsequent release of NO. At 132 °C, TGA-MS revealed the evolution of species of 30 m/z consistent with NO release and continued through the remainder of the experiment (Supplementary Fig. 3). Heating to a final temperature of 145 °C during thermal analysis

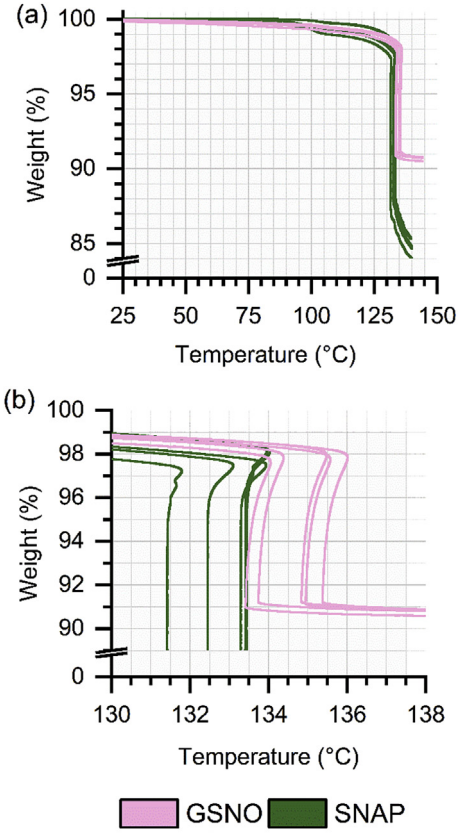

Fig. 2. Stepwise isothermal thermogravimetric analyses of GSNO (pink) and SNAP (green). GSNO and SNAP thermally decompose to release NO at 134.7 ± 0.8 °C and 132.8 ± 0.9 °C, respectively. Data reported as mean ± SD of $n = 5$ replicate measurements. (For interpretation of the references to color in this figure legend, the reader is referred to the Web version of this article.)

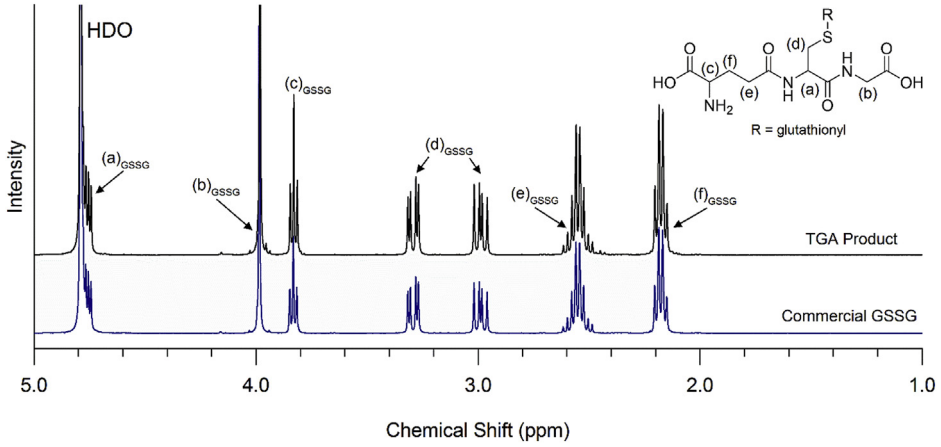

Fig. 3. ^{1}H NMR spectra comparing GSNO TGA product to commercial GSSG. Spectrum acquired in D_2O at 25 °C.

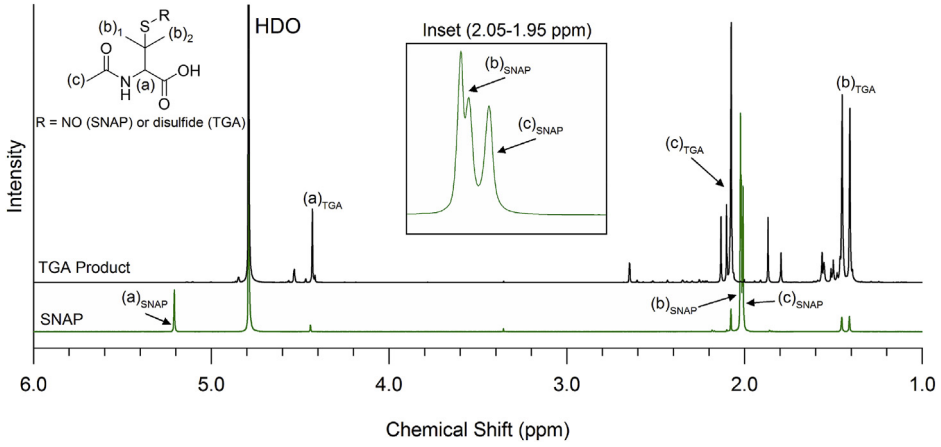

Fig. 4. ^{1}H NMR spectra comparing SNAP TGA product to SNAP. Spectrum acquired in D_2O at 25 °C.

produced a yellow oil that was difficult to collect from the pan. During TGA, SNAP exhibited continuous mass loss after 132 °C (Supplementary Fig. 4), likely due to concurrent melting and decomposition of both SNAP and NAP disulfide. This hypothesis can be inferred from visual observations of the SNAP product, as well as reported melting points of SNAP (152–154 °C) and NAP disulfide (128–131 °C) [26]. In both cases, prior literature indicates melting is accompanied by decomposition. Although these referenced observations are not derived from rigorous thermal analyses, it is clear that a binary mixture of SNAP and NAP disulfide must experience multiple thermal transitions and decomposition processes when heated to 145 °C. When using a lower final temperature of 140 °C, a resinous, light blue-green solid could be recovered and characterized by ATR-FTIR and ^{1}H NMR. ATR-FTIR spectra (Supplementary Fig. 5) revealed the absence of the diagnostic N=O stretching band at 1497 cm^{-1}, supporting decomposition of the RSNO functional group. ^{1}H NMR analysis of the SNAP TGA product (Fig. 4) indicates that thermal decomposition of SNAP primarily yields NAP disulfide, as well as other unidentified compounds that may represent significant products. Accurate-mass TOF-MS was used to confirm the presence of NAP disulfide (379.1020 *m/z*, $[M-H]^-$), as well as homologous tri- and tetrasulfides (411.0734 and 443.0438 *m/z*, $[M-H]^-$) that may contribute to the unknown products detected by ^{1}H NMR (Supplementary Table 1). The presence of these higher sulfides may be rationalized as the outcome of various radical combination events that occur during thermal decomposition [31]. We propose that the NO-producing decomposition of SNAP at 132.8 ± 0.9 °C results in formation of NAP disulfide, which is itself thermally unstable and undergoes further decomposition to produce the series of products observed by MS. This accumulation of products may result in a eutectic mixture that is molten below the 152–154 °C melting range of SNAP and perhaps facilitates more rapid or complex decomposition.

The mean NO-forming decomposition of SNAP (132.8 ± 0.9 °C) occurs at a lower temperature than the equivalent phenomenon in GSNO (134.7 ± 0.8 °C). In solution, it is believed that the rate of RSNO decomposition is influenced by steric considerations during thiyl combination [25], as well as the possibility of both geminate and non-geminate recombination of thiyl and NO radicals [21]. Since these complex reaction equilibria are unlikely to become established during high-temperature thermal decomposition, it is feasible that TGA results reflect a genuine difference in S–N bond stability. On this basis, Bainbrigge et al. reasoned that geminal dimethyl substitution in SNAP did not significantly influence the stability of the S–N bond due to apparently identical decomposition temperatures of 148 °C. Our higher resolution data suggests that SNAP exhibits modestly decreased stability, which may be attributable to tertiary substitution. In any event, it is evident that tertiary substitution influences the electronic environment of the RSNO functional group. In GSNO, the RSNO carbon is primary and exhibits a ^{13}C NMR chemical shift of 34.03 ppm (Supplementary Fig. 6). In SNAP, the dimethyl-substituted tertiary RSNO carbon is shifted downfield to 57.77 ppm and is comparatively electron deficient. A similar deshielding effect has been observed using ^{15}N NMR which indicates that geminal dimethyl substitution exerts a considerable influence on the electronic properties of the RSNO functional group [32].

Table 1
Percent decomposition of RSNOs in the presence and absence of metal ion chelators.

	Average decomposition (%)[a]	
RSNO[b]	Chelator[c]	Without chelator
GSNO[d]	1.4 ± 0.2	2.5 ± 0.2
SNAP[d]	10.8 ± 0.3	98.0 ± 0.1

[a] Average decomposition measured over 24 h. Data reported as mean ± SD of $n \geq 3$ replicate measurements.
[b] RSNO (1.5×10^{-3} M; PBS; pH 7.4).
[c] EDTA (100 μM).
[d] Average decomposition statistically different ($p < 0.01$) in the presence and absence of metal ion chelator by two-tailed Student's t-test.

3.2. Effect of temperature on solution stability

RSNO stability as a function of temperature and pH has been previously examined [22,23,33], but many older studies neglect to account for the presence of trace metal ions which catalyze the decomposition of RSNOs [14]. de Souza et al. report chelation protocols [34]; however, the magnitude of the impact of trace metal ions on RSNO stability is seldom quantified. We conducted an experiment in which the decomposition of GSNO and SNAP was compared in PBS (pH 7.4) prepared in ultrapure water (18.2 MΩ cm) with and without 100 μM EDTA (Table 1). Over 24 h, both RSNOs exhibited statistically greater ($p < 0.01$) decomposition without the chelator in solution, particularly in the case of SNAP, which underwent near complete decomposition. Because the absence of EDTA results in accelerated decomposition even when buffer solutions are prepared with ultrapure water, we hypothesize that metal ions may be introduced by glassware or the RSNOs themselves. The particular sensitivity of SNAP to the absence of EDTA could be explained by a higher concentration of adventitious copper or perhaps a greater inherent susceptibility to decomposition by trace metal ions. Furthermore, it is known that GSNO is capable of chelating and inactivating copper ions in a self-stabilizing manner, which could also account for this difference [2]. The individual components of our experiments were determined to contain ≤0.2 μM copper (method detection limit) by ICP-AES (Supplementary Table 2). It has been reported previously that copper ion concentrations as low as 10^{-5} to 10^{-6} M (typical of buffer components) are capable of decomposing RSNOs [35]. Although we fail to detect copper using ICP-AES, its presence in trace quantities is evidently a factor in the stability of GSNO and SNAP, reinforcing the necessity of trace metal chelation for proper evaluation and use of RSNO solutions.

We evaluated the effect of temperature on the relative stability of 1.5×10^{-3} M solutions of GSNO and SNAP (PBS; pH 7.4) with 100 μM EDTA as the chelating species. The three temperatures tested were 5 °C (refrigeration), 22 °C (room temperature), and 37 °C (physiological) due to their relevance in laboratory settings. Our results indicate increased RSNO stability with decreasing temperature (Fig. 5). At 5 °C, GSNO showed minimal (0.4 ± 0.6%) decomposition over a 7-day period, suggesting light-free refrigeration is sufficient for preserving samples over this timespan. In contrast, SNAP decomposed 2.3 ± 0.3% after 1 day and 11 ± 1% after 1 week, which suggests that solutions of SNAP should be prepared immediately prior to use. After 1 week at 22 °C, GSNO and SNAP exhibited 10 ± 4 and 64 ± 1% decomposition, respectively, revealing an even greater difference in stability between the two RSNOs. At 37 °C, GSNO decomposed 3 ± 1% in a 24 h period and 26 ± 1% over 7 days, whereas SNAP was almost fully decomposed after 2 days (82 ± 1%). Depending on the application, GSNO is apparently more suitable for experiments in which prolonged stability is required under physiological temperatures. In contrast, SNAP in aqueous solution is clearly susceptible to rapid decomposition. The results of these solution-phase stability studies are unremarkable and consistent with our solid-phase TGA experiments, which suggest that the S–N bond in SNAP may be marginally weaker than in GSNO. However, it has been observed elsewhere that SNAP exhibits remarkable resistance to decomposition (< 12% over 8 months) at 37 °C when crystallized within a polymer matrix, an outcome that was attributed to the stabilizing effect of intermolecular hydrogen bonding [36]. We must therefore conclude that the observed stability of SNAP is highly contingent upon phase and local chemical environment, although dissolution in water assuredly accelerates decomposition. Interestingly, our IR data indicates that the N═O stretching frequency of crystalline SNAP is 20 cm^{-1} greater than that of GSNO (1477 cm^{-1}), which may be indicative of a stronger N═O bond. The RSNO functional group is frequently described in terms of the three distinct resonance forms depicted in Fig. 6, and contribution of the S═N bond in structure **I** may rationalize the existence of *syn/anti* conformers that produce the characteristic red-pink color of primary and secondary RSNOs (*syn*) and green tertiary RSNOs (*anti*). Chemical factors that increase the contribution of structure **I** are theorized to impart greater resistance to homolytic cleavage, which is clearly disfavored by the presence of the double bond. The apparent strength of the N═O bond in SNAP suggests that the relative contribution of structure **I** may be reduced compared to GSNO, where hydrogen bonding to the RSNO oxygen may favor the double-bonded form and lower the frequency at which the ν(N═O) mode is observed. However, it is also feasible that ν(N═O) frequency differences are a direct consequence of *syn/anti* conformation and do not provide insight into the local hydrogen bonding environment [37].

In a recent study, de Souza et al. examined the long-term (> 35 days) solution stability of 1×10^{-3} M solutions of the primary RSNOs GSNO and *S*-nitroso-*N*-acetylcysteine (SNAC) in pH 7 PBS containing 0.1 wt% EDTA [34]. Their results support an inverse relationship between temperature and RSNO stability for both RSNOs. They found that GSNO was less stable than SNAC at all tested temperatures (15, 25, 30, 35, and 40 °C) and that both were modestly stable (< 5% decomposition) at 15 °C over several weeks. Interestingly, we observed that SNAP (a tertiary analogue of SNAC) is *less* stable than GSNO in pH 7.4 PBS at 5, 22, and 37 °C, in spite of geminal dimethyl substitution of the RSNO carbon that has been thought to confer additional stability relative to primary RSNOs [23]. Indeed, our combined studies suggest that the order of stability is SNAC > GSNO > SNAP at neutral or near-neutral pH.

To explain the exceptional stability of SNAC, de Souza et al. invoke the formation of a seven-membered ring through hydrogen bonding between the carbonyl oxygen of the acetamido group and the hydrogen atom of the protonated carboxylic acid group [21]. The formation of this seven-membered ring facilitates a favorable hydrogen bonding interaction between the *syn* RSNO oxygen and the amide hydrogen, which acts to stabilize the molecule with respect to NO-forming decomposition. However, this model does not directly address the likelihood that the carboxylic acid group of SNAC will be predominately deprotonated at or above neutral pH. In computational studies, Meyer et al. developed an alternative model in which a *five*-membered ring involving a negatively-charged carboxylate oxygen and the amide hydrogen is favored at physiological pH [38]. This configuration may stabilize SNAC through formation of an unusual hydrogen bond-like interaction between the RSNO oxygen and hydrogen atoms bound to the RSNO carbon, a phenomenon that is impossible in tertiary substrates such as SNAP. In solids, the feasibility of this interaction is potentially supported by crystal structures of *S*-nitrosocaptopril and the ethyl ester of *S*-nitrosocysteine, in which the NO moiety preferentially eclipses a C–H bond of the RSNO carbon [39]. Meyer et al. argued that this interaction may explain preference for the *syn* conformation in primary RSNOs, while *trans* is preferred in tertiary substrates. Furthermore, Meyer et al. identified that both SNAC and SNAP are subject to a chalcogen-chalcogen interaction between the thiyl radical generated as a decomposition intermediate and the neighboring carboxylate group. The magnitude of this interaction was greater in the case of SNAP which may stabilize the sulfur-centered radical and consequently

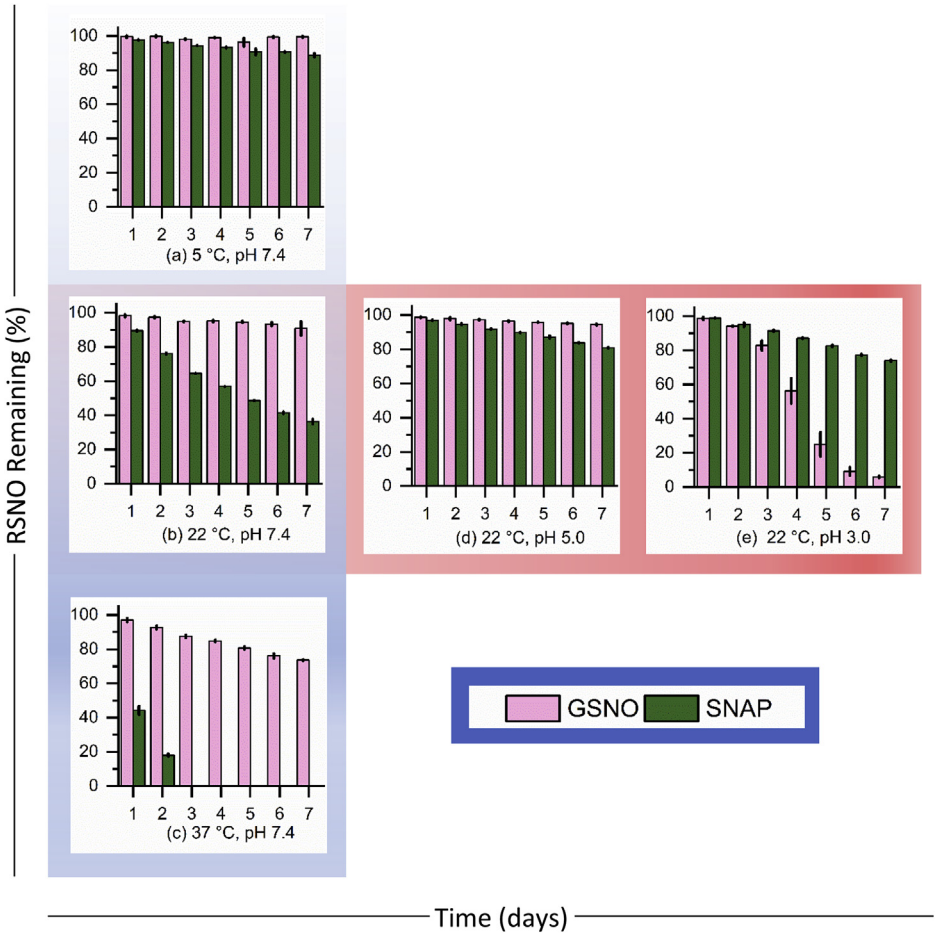

Fig. 5. RSNO solution stability as a function of temperature (PBS) and pH (citric acid/Na_2HPO_4 buffer) at (a) 5 °C, pH 7.4 (b) 22 °C, pH 7.4, (c) 37 °C, pH 7.4 (d) 22 °C, pH 5.0 and (e) 22 °C, pH 3.0. GSNO (1.5×10^{-3} M; monitored at 335 nm) and SNAP (1.5×10^{-3} M; monitored at 339 nm) decay monitored over a one-week period. Data reported as mean ± SD of $n \geq 3$ replicate measurements.

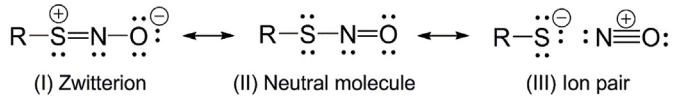

Fig. 6. RSNO resonance structures.

promote decomposition. This model appears to be generally consistent with the reduced stability of SNAP compared to SNAC and may partially rationalize the apparent stability of GSNO. If the proposed hydrogen bonding interaction between the RSNO oxygen and hydrogen atoms bound to the RSNO carbon is the major factor that determines *syn/anti* configuration, then GSNO may also experience this interaction. This possibility is supported by the red-pink color of GSNO, which arises from an absorbance maximum at 545 nm ($n_N \rightarrow \pi^*$) that is attributable to the electronic properties of the *syn* conformer. Furthermore, GSNO lacks neighboring carboxylate groups to stabilize intermediate thiyl radicals. We hypothesize that a combination of the intramolecular effects described by Meyer et al. and the ability of GSNO to chelate copper ions are largely responsible for its greater stability relative to SNAP. Curiously, we observed that the red-pink color of GSNO is retained when cooled with liquid nitrogen, while SNAP loses its green color and develops a vivid pink appearance (Supplementary Fig. 7). This property is not shared with *S*-nitroso-triphenylmethanethiol, a tertiary RSNO that remains green when cooled in an identical manner. We propose that this observation may be indicative of an unexpected temperature-dependent conformational change in SNAP from *anti* to *syn*, although the apparent color change may also represent a conformationally-unrelated hypsochromic shift of the $n_N \rightarrow \pi^*$ transition at 591 nm or another purely electronic or optical phenomenon.

3.3. Effect of pH on solution stability

The majority of studies examining the influence of pH on RSNO stability hypothesize that RSNOs exhibit enhanced solution stability in acidic media [13,22,23] while one study reports enhanced stability in mildly basic media [33]. To address this apparent discrepancy, we used GSNO and SNAP to assess the comparative stability of RSNOs at physiological (PBS; pH 7.4) and mildly acidic (citric acid/Na_2HPO_4 buffer; pH 5.0 and 3.0) pH over 7 days. The results of this pH variation study are presented in Fig. 5. Compared with experiments performed at pH 7.4, GSNO and SNAP exhibit an appreciable increase in stability at pH 5.0. Acidic conditions may stabilize RSNOs by protonation of the RSNO oxygen, leading to enhanced *S*–N bond strength via resonance, as depicted in Fig. 6(I) [21–24]. However, a further decrease in pH to 3.0 demonstrated that SNAP is *less* stable than at pH 5.0 ($p < 0.01$). In the case of GSNO, a distinct decomposition phenomenon manifests at pH 3.0. Over 2 days, GSNO shows a similar linear decomposition rate to that of SNAP. However, from 3 to 7 days, GSNO exhibited a rapid increase in decomposition as indicated in Fig. 5e. This unusual decomposition behavior was also observed when EDTA was replaced with 1 w/v % Chelex 100, a solid phase iminodiacetic acid chelating resin active in strongly basic to weakly acidic solutions (Supplementary Fig. 8) [40]. The possibility that copper is directly responsible for the increased rate of decomposition at pH 3.0 is unlikely, considering that the effect requires several days to manifest and does not extend to SNAP. One hypothesis for this irregular behavior is that peptide bonds in GSNO are slowly hydrolyzed at pH 3.0, ultimately resulting in decay of the entire molecule. However, peptide bonds are reasonably stable, and hydrolysis by 6 M HCl at 110 °C is a slow process [41]. A second hypothesis is that GSNO exhibits autocatalytic decomposition at pH 3.0,

indicated by the possible sigmoidal decay behavior. Potential factors capable of inducing this rapid decay are oxygenated conditions or the presence of thiols in solution. One possible aerobic mechanism is N_2O_3-catalyzed decomposition resulting from reaction of NO and oxygen [42]. Oxygenated conditions have also been proposed to effect nitrosonium-catalyzed decomposition, which is perhaps enhanced at low pH where the production of nitrosonium is likely more favorable [20]. Thiols such as GSH may accelerate decomposition by reducing Cu^{2+} to Cu^{+}, the active form of copper in the metal ion-mediated RSNO decomposition mechanism [12,14]. To assess these hypotheses, we performed experiments under anaerobic conditions and with the addition of *N*-ethylmaleimide (NEM) as a thiol scavenger (Supplementary Table 3). We found that GSNO exhibited similar, if not more rapid, decomposition behavior in the presence of NEM. Interestingly, in the absence of oxygen GSNO was more stable and exhibited linear decomposition. This observation may be explained as the inhibition of autocatalytic decomposition under anaerobic conditions [42,43]. As described by Grossi et al., the formation of N_2O_3 may catalyze the rapid decomposition of RSNOs [42]. The rate of this N_2O_3-mediated chain reaction decreases as the substituents of the RSNO carbon increase in steric bulk, suggesting that GSNO (primary) may be more inherently susceptible to this pathway than SNAP (tertiary) in a manner consistent with our observations. Because N_2O_3 exists in equilibrium with nitrous acid (the immediate oxidation product of NO; pK_a 3.16), it seems reasonable to hypothesize that this pathway is particularly influential at lower pH values and therefore manifests in our study at pH 3.0 [44,45]. In a related study using the same citric acid/Na_2HPO_4 buffer system, de Souza et al. observed that GSNO exhibited first-order exponential decay kinetics at pH 3 [34]. After 10 days, GSNO appeared to be fully decomposed, which aligns reasonably well with our observation that GSNO was almost fully decomposed by 7 days. However, de Souza et al. observed greater comparative GSNO stability at pH 7 than pH 5 over a period of 30 days, while we observe that GSNO is marginally more stable at pH 5.0 over 7 days. To explain this phenomenon, de Souza et al. argue somewhat tautologically that the biological role of GSNO may obligate increased stability at physiological pH. We note that a modest increase in RSNO stability is a predicted effect of acidic conditions, in line with our own observations of both GSNO and SNAP. In any case, the solution stability of RSNOs in mildly acidic or physiological media is likely to be influenced by a variety of factors, including solvent, the presence of ionizable functional groups, and resulting intra- and intermolecular hydrogen bonding interactions.

3.4. Solution stability with fluorescent light exposure

Although susceptibility of RSNOs to photolytic decomposition has been established, short-term exposure of RSNOs to laboratory lighting is rarely considered a major concern. In fact, it has been advised that the photolytic vulnerability of RSNOs is minimal in the absence of strong, direct light and that particular caution is necessary only in pharmacological studies [17]. Since preparation, handling, and use of RSNO solutions may amount to multiple hours of light exposure, we conducted photolytic decomposition studies over 7 h to evaluate the stability of GSNO and SNAP under laboratory lighting conditions in a hood (d = 122 cm, 861 lux) in a typical workday. The fluorescent light emits wavelengths from 425 nm to 650 nm (Supplementary Fig. 9). Both GSNO and SNAP were highly susceptible to photolytic decomposition from this light source, as shown in Fig. 7. RSNOs have two characteristic absorption bands, one in the 330–335 nm range and one in the 550–600 nm range [13]. The spectrum of the fluorescent light source strongly overlaps with the RSNO absorption band in the visible light region, which is known to accelerate RSNO decomposition [46]. After only 1 h of light exposure, the concentration of 1.5×10^{-3} M GSNO solutions (PBS; pH 7.4) had decreased to 97.9 ± 1.0% of the original value, while SNAP exhibited a comparable decrease to 95.6 ± 0.1%. Both RSNO solutions continued to decompose linearly in proportion to exposure time, with SNAP exhibiting greater susceptibility to visible light-induced decomposition (69.7 ± 1.6% remaining after 7 h) compared to GSNO (80.8 ± 0.5% remaining after 7 h) ($p < 0.01$). For comparison, GSNO decomposed 98.2 ± 0.8% and SNAP decomposed 89.5 ± 0.5% over 24 h in the absence of light under the same conditions. These results show that, even over a 1 h timescale, minimizing lab lighting and utilizing amber glassware is important for maintaining RSNO solution purity. Further considerations include usage of dark rooms or high wavelength (> 600 nm) lighting (Supplementary Fig. 10) when handling RSNO samples.

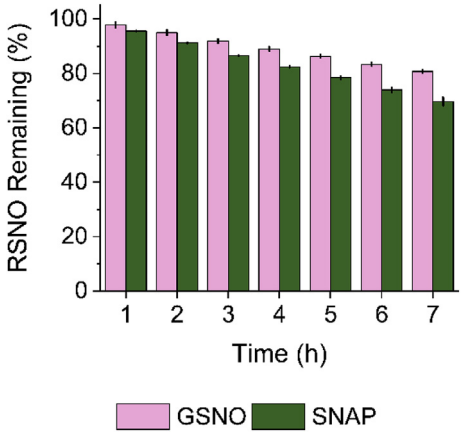

Fig. 7. RSNO solution stability as a function of fluorescent light exposure. GSNO (1.5×10^{-3} M; PBS; pH 7.4; monitored at 335 nm) and SNAP (1.5×10^{-3} M; PBS; pH 7.4; monitored at 339 nm) decay monitored over 7 h with source to sample distance of d = 122 cm (861 lux). Data reported as mean ± SD of $n \geq 3$ replicate measurements.

4. Conclusions

In all but one circumstance, GSNO displayed greater stability than SNAP. Data collected from TGA experiments indicated that both RSNOs release NO at temperatures 15 °C below what has been previously reported in the literature. Notably, the thermal decomposition temperatures at which homolytic cleavage of the S–N bond occurs for GSNO (134.7 ± 0.8 °C) and SNAP (132.8 ± 0.9 °C) were significantly different. GSNO decomposed to yield GSSG stoichiometrically, whereas decomposition of SNAP produced NAP disulfide and tri- and tetrasulfides. In the presence of metal ion chelators in solution, GSNO is stable enough to be stored in a refrigerator for at least 1 week with negligible decomposition. In contrast, it is recommended that SNAP be prepared daily. Additionally, for studies at physiological temperature and pH, SNAP is preferred for uses that require rapid NO release and GSNO is preferred for uses that require greater stability. If storage at room temperature is preferred or required, decreasing the pH of solutions of GSNO and SNAP to 5.0 would increase stability and prolong the shelf life. The most important consideration, arguably, is the effect of fluorescent laboratory lighting on the stability of RSNOs. Both GSNO and SNAP were appreciably sensitive to photolytic decomposition on an hourly timescale, highlighting the need for effective light shielding techniques during preparation and storage. Further studies are warranted to elucidate the conditions for optimal stability of these RSNOs.

Disclosure statement

The authors declare no conflicts of interest.

Acknowledgements

A. C. M. was supported by the National Science Foundation (DGE-1450032). C. L. A. was supported by the National Institutes of Health

(5R01HL140301-02).

Appendix A. Supplementary data

Supplementary data to this article can be found online at https://doi.org/10.1016/j.niox.2019.08.002.

References

[1] D. Giustarini, A. Milzani, R. Colombo, I. Dalle-Donne, R. Rossi, Nitric oxide and *S*-nitrosothiols in human blood, Clin. Chim. Acta 330 (2003) 85–98, https://doi.org/10.1016/S0009-8981(03)00046-9.

[2] K.A. Broniowska, A.R. Diers, N. Hogg, S-nitrosoglutathione, Biochim. Biophys. Acta 1830 (2013) 3173–3181, https://doi.org/10.1016/j.bbagen.2013.02.004.

[3] K.A. Broniowska, N. Hogg, The chemical biology of S-nitrosothiols, antioxid, Redox Signal. 17 (2012) 969–980, https://doi.org/10.1089/ars.2012.4590.

[4] T.C. Major, D.O. Brant, C.P. Burney, K.A. Amoako, G.M. Annich, M.E. Meyerhoff, H. Handa, R.H. Bartlett, The hemocompatibility of a nitric oxide generating polymer that catalyzes *S*-nitrosothiol decomposition in an extracorporeal circulation model, Biomaterials 32 (2011) 5957–5969, https://doi.org/10.1016/j.biomaterials.2011.03.036.

[5] T.C. Major, H. Handa, E.J. Brisbois, M.M. Reynolds, G.M. Annich, M.E. Meyerhoff, R.H. Bartlett, The mediation of platelet quiescence by NO-releasing polymers via cGMP-induced serine 239 phosphorylation of vasodilator-stimulated phosphoprotein, Biomaterials 34 (2013) 8086–8096, https://doi.org/10.1016/j.dcn.2011.01.002 (The).

[6] S.P. Hopkins, J. Pant, M.J. Goudie, C. Schmiedt, H. Handa, Achieving long-term biocompatible silicone via covalently immobilized *S*-nitroso-*N*-acetylpenicillamine (SNAP) that exhibits 4 Months of sustained nitric oxide release, ACS Appl. Mater. Interfaces 10 (2018) 27316–27325, https://doi.org/10.1021/acsami.8b08647.

[7] E.J. Brisbois, H. Handa, M.E. Meyerhoff, Recent advances in hemocompatible polymers for biomedical applications, Adv. Polym. Med, Springer, Cham, 2015, pp. 481–511, , https://doi.org/10.1007/978-3-319-12478-0_16.

[8] E.J. Brisbois, H. Handa, T.C. Major, R.H. Bartlett, M.E. Meyerhoff, Long-term nitric oxide release and elevated temperature stability with *S*-nitroso-*N*-acetylpenicillamine (SNAP)-doped Elast-eon E2As polymer, Biomaterials 34 (2013) 6957–6966, https://doi.org/10.1016/j.biomaterials.2013.05.063.

[9] B.H. Neufeld, M.M. Reynolds, Critical nitric oxide concentration for *Pseudomonas aeruginosa* biofilm reduction on polyurethane substrates, Biointerphases 11 (2016) 031012, https://doi.org/10.1116/1.4962266.

[10] S. Giri, R. Rattan, M. Deshpande, J.L. Maguire, Z. Johnson, R.P. Graham, V. Shridhar, Preclinical therapeutic potential of a nitrosylating agent in the treatment of ovarian cancer, PLoS One 9 (2014) 1–11, https://doi.org/10.1371/journal.pone.0097897.

[11] N. Gould, P.T. Doulias, M. Tenopoulou, K. Raju, H. Ischiropoulos, Regulation of protein function and signaling by reversible cysteine *S*-nitrosylation*, J. Biol. Chem. 288 (2013) 26473–26479, https://doi.org/10.1074/jbc.R113.460261.

[12] A.P. Dicks, H.R. Swift, D.L.H. Williams, A.R. Butler, H.H. Al-Sa'doni, B.G. Cox, Identification of Cu^{+} as the effective reagent in nitric oxide formation from *S*-nitrosothiols (RSNO), J. Chem. Soc. Perkin Trans. 2 (1996) 481–487.

[13] D.L.H. Williams, The chemistry of S-nitrosothiols, Acc. Chem. Res. 32 (1999) 869–876, https://doi.org/10.1021/ar9800439.

[14] R.J. Singh, N. Hogg, J. Joseph, B. Kalyanaraman, Mechanism of nitric oxide release from *S*-nitrosothiols, Biochemistry 271 (1996) 18596–18603, https://doi.org/10.1074/jbc.271.31.18596.

[15] Y. Wu, F. Zhang, Y. Wang, M. Krishnamoorthy, P. Roy-Chaudhury, B.E. Bleske, M.E. Meyerhoff, Photoinstability of *S*-nitrosothiols during sampling of whole blood: a likely source of error and variability in *S*-nitrosothiol measurements, Clin. Chem. 54 (2008) 916–918, https://doi.org/10.1373/clinchem.2007.102103.

[16] J. Pant, M.J. Goudie, S.P. Hopkins, E.J. Brisbois, H. Handa, Tunable nitric oxide release from *S*-nitroso-*N*-acetylpenicillamine via catalytic copper nanoparticles for biomedical applications, ACS Appl. Mater. Interfaces 9 (2017) 15254–15264, https://doi.org/10.1021/acsami.7b01408.

[17] N. Hogg, Biological chemistry and clinical potential of S-nitrosothiols, Free Radic. Biol. Med. 28 (2000) 1478–1486, https://doi.org/10.1016/S0891-5849(00)00254-9.

[18] B. Blanchard, C. Servy, C. Ducrocq, Chemical evaluation of compounds as nitric oxide or peroxynitrite donors using the reactions with serotonin, Free Radic. Res. 34 (2001) 189–191.

[19] J.S. Stamler, E.J. Toone, The decomposition of thionitrites, Curr. Opin. Chem. Biol. 6 (2002) 779–785, https://doi.org/10.1016/S1367-5931(02)00383-6.

[20] Y.L. Zhao, P.R. McCarren, K.N. Houk, B.Y. Choi, E.J. Toone, Nitrosonium-catalyzed decomposition of *S*-nitrosothiols in solution: a theoretical and experimental study, J. Am. Chem. Soc. 127 (2005) 10917–10924, https://doi.org/10.1021/ja050018f.

[21] M.G. de Oliveira, S.M. Shishido, A.B. Seabra, N.H. Morgon, Thermal stability of primary *S*-nitrosothiols: roles of autocatalysis and structural effects on the rate of nitric oxide release, J. Phys. Chem. A 106 (2002) 8963–8970, https://doi.org/10.1021/jp025756u.

[22] L. Heikal, G.P. Martin, L.A. Dailey, Characterisation of the decomposition behaviour of S-nitrosoglutathione and a new class of analogues: S-Nitrosophytochelatins, Nitric Oxide 20 (2009) 157–165, https://doi.org/10.1016/j.niox.2008.11.001.

[23] B. Roy, A. du Moulinet d'Hardemare, M. Fontecave, New thionitrites: synthesis, stability, and nitric oxide generation, J. Org. Chem. 59 (1994) 7019–7026, https://doi.org/10.1021/jo00102a028.

[24] Q.K. Timerghazin, G.H. Peslherbe, A.M. English, Resonance description of *S*-nitrosothiols: insights into reactivity, Org. Lett. 9 (2007) 3049–3052, https://doi.org/10.1021/ol0711016.

[25] N. Bainbrigge, A.R. Butler, C.H. Görbitz, The thermal stability of *S*-nitrosothiols: experimental studies and *ab initio* calculations on model compounds, J. Chem. Soc. Perkin Trans. 2 (1997) 351–353, https://doi.org/10.1039/a604148e.

[26] L. Field, R.V. Dilts, R. Ravichandran, P.G. Lenhert, G.E. Carnahan, An unusually stable thionitrite from *N*-Acetyl-D,L-penicillamine; X-ray crystal and molecular structure of 2-(Acetylamino)-2-carboxy-l,ldimethylethyl thionitrite, J. Chem. Soc., Chem. Commun. (1978) 249–250.

[27] H.A. Moynihan, S.M. Roberts, Preparation of some novel *S*-nitroso compounds as potential slow-release agents of nitric oxide in vivo, J. Chem. Soc. Perkin Trans. 1 (1994) 797–805.

[28] T.W. Hart, Some observations concerning the S-nitroso and S-phenylsulphonyl derivatives of L-cysteine and glutathione, Tetrahedron Lett. 26 (1985) 2013–2016, https://doi.org/10.1016/S0040-4039(00)98368-0.

[29] M. Parent, F. Dahboul, R. Schneider, I. Clarot, P. Maincent, P. Leroy, A. Boudier, A complete physicochemical identity card of *S*-nitrosoglutathione, Curr. Pharmaceut. Anal. 9 (2013) 31–42, https://doi.org/10.2174/157341213804806098.

[30] TA Instruments, High resolution thermogravimetric analysis - a new technique for obtaining superior analytical results, Therm. Anal. Rheol. TA-023 (n.d.).

[31] R.S. Asquith, L. Hirst, The photochemical degradation of cystine in aqueous solution in the presence of air, Biochim. Biophys. Acta 184 (1969) 345–357, https://doi.org/10.1016/0304-4165(69)90037-3.

[32] K. Wang, Y. Hou, W. Zhang, M.B. Ksebati, M. Xian, J.P. Cheng, P.G. Wang, ^{15}N NMR and electronic properties of *S*-nitrosothiols, Bioorg. Med. Chem. Lett 9 (1999) 2897–2902, https://doi.org/10.1016/S0960-894X(99)00499-0.

[33] I. Hornyák, K. Marosi, L. Kiss, P. Gróf, Z. Lacza, Increased stability of *S*-nitrosothiol solutions via pH modulations, Free Radic. Res. 46 (2012) 214–225.

[34] G.F.P. de Souza, J.P. Denadai, G.F. Picheth, M.G. de Oliveira, Long-term decomposition of aqueous S-nitrosoglutathione and S-nitroso-N-acetylcysteine: influence of concentration, temperature, pH and light, Nitric Oxide 84 (2019) 30–37, https://doi.org/10.1016/j.niox.2019.01.002.

[35] D.L.H. Williams, The mechanism of nitric oxide formation from *S*-nitrosothiols (thionitrites), Chem. Commun. (1996) 1085–1091, https://doi.org/10.1002/chin.199644254.

[36] Y. Wo, Z. Li, E.J. Brisbois, A. Colletta, J. Wu, T.C. Major, C. Xi, R.H. Bartlett, A.J. Matzger, M.E. Meyerhoff, Origin of long-term storage stability and nitric oxide release behavior of CarboSil polymer doped with *S*-nitroso-*N*-acetyl-D-penicillamine, ACS Appl. Mater. Interfaces 7 (2015) 22218–22227, https://doi.org/10.1021/acsami.5b07501.

[37] A. Canneva, M.F. Erben, R.M. Romano, Y.V. Vishnevskiy, C.G. Reuter, N.W. Mitzel, C.O. Della Védova, The structure and conformation of $(CH_3)_3CSNO$, Chem. Eur J. 21 (2015) 10436–10442, https://doi.org/10.1002/chem.201500811.

[38] B. Meyer, A. Genoni, A. Boudier, P. Leroy, M.F. Ruiz-Lopez, Structure and stability studies of pharmacologically relevant *S*-nitrosothiols: a theoretical approach, J. Phys. Chem. A 120 (2016) 4191–4200, https://doi.org/10.1021/acs.jpca.6b02230.

[39] J. Yi, M.A. Khan, J. Lee, G.B. Richter-Addo, The solid-state molecular structure of the *S*-nitroso derivative of L-cysteine ethyl ester hydrochloride, Nitric Oxide 12 (2005) 261–266, https://doi.org/10.1016/j.molcel.2008.04.008.Comprehensive.

[40] Bio-Rad Laboratories, Chelex 100 and Chelex 20 Chelating Ion Exchange Resin Instruction Manual, (n.d).

[41] A.S. Inglis, P.W. Nicholls, C.M. Roxburgh, Hydrolysis of the peptide bond and amino acid modification with hydriodic acid, Austrailian J. Biol. Sci. 24 (1971) 1235–1240.

[42] L. Grossi, P.C. Montevecchi, A kinetic study of *S*-nitrosothiol decomposition, Chem. Eur J. 8 (2002) 380–387.

[43] L. Grossi, P.C. Montevecchi, S. Strazzari, Decomposition of *S*-nitrosothiols: unimolecular versus autocatalytic mechanism, J. Am. Chem. Soc. 123 (2001) 4853–4854, https://doi.org/10.1021/ja005761g.

[44] G.Y. Markovits, S.E. Schwartz, L. Newman, Hydrolysis equilibrium of dinitrogen trioxide in dilute acid solution, Inorg. Chem. 20 (1981) 445–450, https://doi.org/10.1021/ic50216a025.

[45] G. da Silva, E.M. Kennedy, B.Z. Dlugogorski, Ab initio procedure for aqueous-phase p*K*a calculation: the acidity of nitrous acid, J. Phys. Chem. A 110 (2006) 11371–11376, https://doi.org/10.1021/jp0639243.

[46] D.J. Sexton, A. Muruganandam, D.J. McKenny, B. Mutus, Visible light photochemical release of nitric oxide from *S*-nitrosoglutathione: potential photochemotherapeutic applications, Photochem. Photobiol. 59 (1994) 463–497.